Supporting Information for Publication

Tunable spin textures in polar antiferromagnetic hybrid organic-inorganic perovskites by electric and magnetic fields

Feng Lou[1,2,†], Teng Gu[1,2,†], Junyi Ji,[1,2] Junsheng Feng,[3] Hongjun Xiang[1,2,*], and Alessandro Stroppa[4,*]

[1]*Key Laboratory of Computational Physical Sciences (Ministry of Education), State Key Laboratory of Surface Physics, and Department of Physics, Fudan University, Shanghai 200433, China.*
[2]*Collaborative Innovation Center of Advanced Microstructures, Nanjing 210093, China.*
[3]*School of Physics and Materials Engineering，Hefei Normal University, Hefei 230601, P. R. China* [4]*CNR-SPIN, c/o Department of Physical and Chemical Sciences, University of L'Aquila, 67100 Coppito (AQ), L'Aquila, Italy;*

Email: hxiang@fudan.edu.cn, alessandro.stroppa@spin.cnr.it

Contents

Supplementary Note

Supplementary Note 1: The ferroelectric property of $(Me_3NCH_2X)MnY_3$.

In order to evaluate the polarization of TMCM-$MnCl_3$ (TMCM=$(CH_3)_3NCH_2Cl^+$) accurately, we adopt the modern theory of polarization as detailed in the text. We fix two organic cations and rotate the other two in order to simulate the nonpolar-polar transition. There are many different paths which can be exploited to simulate this AFE-FE phase transition. In our work, we adopt the rotation axis along [010] direction, *i.e. b* axis. As shown in Fig. S1, we use the dimensionless parameter λ to describe the AFE-FE path in the configuration space. Note that this dimensionless parameter λ is not the usual linear interpolation for atomic positions but specifies the rotation of cations as well as the displacive-type distortion of the $MnCl_3$ framework. Since this path in the configuration space acts only as a computational tool to exclude the spurious inclusion of quanta of polarization, for each λ we do not optimize the atomic positions but we can evaluate the polarization in order to monitor its continuous evolution as a function of λ. It is understood that only the state with λ=1 has a real physical meaning. We can see a nonmonotonic behavior as a function of λ which is quite common in the case of HOIP ferroelectric. In order-disorder and displacive-type HOIP ferroelectrics, the two different sub-systems, *i.e*. organic cations and inorganic framework, are interacting through hydrogen bonding thus giving rise to a rather complex interplay responsible for the non-monotonic behavior of polarization as a function of λ. In our TMCM-$MnCl_3$ system, all the intermediate states are good insulator. We find P_x is about 4.18 μC/cm^2 and P_z is about -4.48 μC/cm^2 (see Fig. S2), which is in agreement with the experimental value of P_z ~ 4.00 μC/cm^2 by You *et al*.

Considering that the halogen atoms have similar chemical properties, but different electronegativity, it will be an interesting question to see whether the substitution of halogen atoms can effectively modify the electronic dielectric properties. Indeed, by replacing the Cl with Br or I, it is expected that the overall

electronegativity of the halogen atom tends to decrease, thus changing the hydrogen bonding network, *i.e.*, implying a complex atomic redistribution of the organic cations as well as the inorganic framework. At the same time, the electric polarization is modified. For comparison, we take three different substitutions into consideration:

1. Replace the halogen atom in the inorganic framework, that is, for $(Me_3NCH_2X)MnY_3$, X=Cl while Y=F, Cl, Br, or I;

2. Replace the halogen atom on the organic cation, that is, for $(Me_3NCH_2X)MnY_3$, Y=Cl while X=F, Cl, Br, or I;

3. Replace the halogen atoms both on the inorganic framework and organic cation simultaneously, that is, for $(Me_3NCH_2X)MnY_3$, X=Y=F, Cl, Br, or I.

For each case, we fully optimize the lattice constants and atomic positions. The evaluated polarizations are shown in Fig. S2, where the horizontal axis represents the different substitutions of halogen elements and the vertical axis is the polarization including the P_x, P_z, and total polarization P_{tot}. Note that the calculated P_z is always negative. To simplify the discussion, we only report the modulus value of the polarization. We identify the general trend as follows. P_x and P_{tot} always decreases from F to I. That is to say, $(Me_3NCH_2F)MnF_3$ has the largest polarization, wherein the maximum value of P_x is 7.27 $\mu C/cm^2$, and the maximum value of P_{tot} is 8.05 $\mu C/cm^2$. For P_z, the situation is slightly different. In detail, P_z increases first from F to Cl, then decreases from Cl to I, *i.e.*, $(Me_3NCH_2Cl)MnCl_3$ has the maximum value of P_z about 4.46 $\mu C/cm^2$. Our results demonstrate that halogen substitutions have a significant effect on the polarization. Therefore, our calculations suggest that tuning the hydrogen bonding through halogen substitution can be new source for modifying the ferroelectric polarization in HOIPs.

In order to gain insights into the FE microscopic mechanism, we perform symmetry mode decomposition with respect to the paraelectric phase. We find that the polarizations have two contributions, one is from the dipole of organic cation and

the other is from the distortion of the inorganic framework. Besides, we take $(Me_3NCH_2X)MnCl_3$ (where X = F, Cl, Br and I) as example to show how the halogen substitutions can affect the two contributions to the polarization. Considering the effect of stress, we calculate the polarization by fixing or relaxing the unit cell (see Fig. S3). We find that the two optimization strategies give the same results. From F to I, the contributions of organic cations increase monotonously while the contributions of the inorganic framework decrease. Their competitive effects lead to the non-monotonous trend of total polarization. In summary, our calculations show that TMCM-$MnCl_3$ is a prototype of order-disorder and displacement-type ferroelectric, whose polarizations can be tuned by the halogen substitutions.

Supplementary Note 2: The group theory analysis of band degeneracy at Γ point.

The band degeneracy of magnetic system with spin-orbit coupling (SOC) effect can be determined by the dimension of its corresponding double valued magnetic space group co-representation (see Supplementary Table 1). At Γ point, we can ignore the translation part of space group, since it cannot produce the extra phase factor, i.e. we can consider only the point group of the crystal. The magnetic little point group can be written as: $M = G + AG$, where G is a unitary subgroup with index 2 and A is an anti-unitary element in *M*-*G*. Then $\bar{D}_i$, the double valued co-representation of M, can be derived from $\bar{\Delta}_i$, the double valued irreducible representation (IR) of G. For co-presentation, Dimmock Wheeler (DW) rule reads:

$$\sum_{B \in AG} Tr\left(\Delta(B^2)\right) = \begin{cases} +\lambda|G|, type(a) \\ -\lambda|G|, type(b) \\ 0\ , type(c) \end{cases}$$

$\lambda = 1$ for single valued co-representation, while $\lambda = -1$ for double valued co-representation. For $type(a)$, co-representation D_i is reducible and after

reduction, its dimension is equal to the dimension of its corresponding IR of Δ_i. For $type(b)$ and $type(c)$, co-representation D_i is irreducible and its dimension is twice as much as the dimension of Δ_i.

For G-type AFM$_y$ state, $M = \{E, m, T, Tm\}$, $G = C_s = \{E, m\}, A = \{T\}$. The irreducible representations (IRs) of $C_s = \{E, m\}$ is shown in Supplementary Table 2. For double valued co-representations $\bar{D}_3$ and $\bar{D}_4$, $\lambda = -1$, there are four anti-unitary operators $TE, Tm, T\bar{E}, T\bar{m}$.

$$\sum_{B \in AG} Tr\left(\bar{\Delta}_i(B^2)\right)$$

$$= Tr\left(\bar{\Delta}_i((TE)^2)\right) + Tr\left(\bar{\Delta}_i((Tm)^2)\right) + Tr\left(\bar{\Delta}_i((T\bar{E})^2)\right) + Tr\left(\bar{\Delta}_i((T\bar{m})^2)\right), i = 3,4$$

$$= Tr\left(\bar{\Delta}_i(E)\right) + Tr\left(\bar{\Delta}_i(\bar{E})\right) + Tr\left(\bar{\Delta}_i(E)\right) + Tr\left(\bar{\Delta}_i(\bar{E})\right), i = 3,4$$

$$= 0$$

According to the DW rules, $\bar{D}_i, i = 3,4$ belong to the $type(c)$. Since $\bar{\Delta}_i$ are 1-dimensional, $\bar{D}_i$ are 2-dimensional, which means the energy band must be double degenerated at Γ point.

For C-type AFM$_y$ state, $M = \{E, Tm\}, G = C_1 = \{E\}$. The irreducible representations (IRs) of $C_1 = \{E\}$ is shown in Supplementary Table 3. For double valued co-representation $\bar{D}_2$, $\lambda = -1$, there are two anti-unitary operators $Tm, T\bar{m}$.

$$\sum_{B \in AG} Tr\left(\bar{\Delta}_2(B^2)\right)$$

$$= Tr\left(\bar{\Delta}_2((Tm)^2)\right) + Tr\left(\bar{\Delta}_2((T\bar{m})^2)\right)$$

$$= Tr\left(\bar{\Delta}_2(\bar{E})\right) + Tr\left(\bar{\Delta}_2(\bar{E})\right)$$

$$= -2$$

According to the DW rules, $\bar{D}_2$ belongs to the type(a). Since $\bar{\Delta}_2$ is 1-dimensional, $\bar{D}_2$ is also 1-dimensional, resulting no degeneracy at Γ point.

Supplementary Note 3: The continuous manipulation of PST by rotating the magnetic ordering.

For G-type AFM state with different orientations, as long as the spin moments lie in the *ac* plane (*i.e.*, within the $\hat{m}_{ac}$ mirror), they have same magnetic symmetry of $\hat{M} = \{\{E|0\}, \left\{\hat{m}_{ac}\middle|\frac{c}{2}\right\}, \hat{T}\left\{\hat{m}_{ac}\middle|\frac{a+b+c}{2}\right\}, \hat{T}\left\{E\middle|\frac{c}{2}\right\}\}$. It is the same as G-type AFM_y state but with different glide plane. According to the symmetry analysis discussed in the main text, the band structure is double degenerate at Γ point. To figure out the variation of spin texture with different orientations, we choose three typical AFM states labeled by AFM_x, AFM_{xz}, and AFM_z. They represent the states with AFM order parameter of $\mathbf{L_G} \sim \boldsymbol{x}$, $\mathbf{L_G} \sim \boldsymbol{xz}$, and $\mathbf{L_G} \sim \boldsymbol{z}$. That is to say, we rotate the AFM_x state around *b* axis by 45°, we can get AFM_{xz} state. Another rotation by 45° can lead to the AFM_z state. The band structures without SOC and with SOC are shown in Fig. 6. One can see the rotation of magnetic ordering has little effect on the band structure and it is double degenerate at Γ point (see Fig. 6b-6d). To illustrate the variation of spin textures, we choose different sections to draw spin textures. As shown in Fig. S7, we adopt the section containing k_a and k_b to draw the spin texture of $\mathbf{L_G} \sim \boldsymbol{x}$. In Fig. S8, we adopt the section containing k_{ac} and k_b to draw the spin texture of $\mathbf{L_G} \sim \boldsymbol{xz}$. In Fig. S9, we adopt the section containing k_c and k_b to draw the spin texture of $\mathbf{L_G} \sim \boldsymbol{z}$. Here k_a, k_b, k_c, and k_{ac} denote the k path from (0,0,0) to (0.5,0,0), (0,0.5,0), (0,0,0.5), and (0.5,0,0.5) with the unit of $\mathrm{Å}^{-1}$, respectively. We can see the PST not only at VBM but also at CBM in all these states and surprisingly the PST can be continuously manipulated by switching the magnetic ordering.

Supplementary Tables

Supplementary Table 1. The symmetry operations and the band degeneracy at Γ point. The magnetic little point group at Γ point is presented by *M=G+AG*, where *G* is a unitary subgroup with index 2 and A is an anti-unitary element in *M-G*. $\overline{\Delta}_i$ are double valued IRs of *G*. $\overline{D}_i$ are double valued co-representations derived from $\overline{\Delta}_i$.

	G-type AFM$_y$		**C-type AFM$_y$**
Magnetic symmetry	$\{E\|0\}, \left\{\hat{m}_{ac}\middle\|\frac{a+b+c}{2}\right\}$ $\hat{T}\left\{E\middle\|\frac{a+b}{2}\right\}, \hat{T}\left\{\hat{m}_{ac}\middle\|\frac{c}{2}\right\}$		$\{E\|0\}, \left\{E\middle\|\frac{a+b}{2}\right\}$ $\hat{T}\left\{\hat{m}_{ac}\middle\|\frac{a+b+c}{2}\right\}, \hat{T}\left\{\hat{m}_{ac}\middle\|\frac{c}{2}\right\}$
M	$\{E, m, T, Tm\}$		$\{E, Tm\}$
G	$C_s = \{E, m\}$		$C_1 = \{E\}$
A	T		Tm
$\overline{\Delta}_i$	$\overline{\Delta}_3$	$\overline{\Delta}_4$	$\overline{\Delta}_2$
Dimension of $\overline{\Delta}_i$	1		
Double valued co-representation type	c		a
Degeneracy (Dimension of $\overline{D}_i$)	2		1

Supplementary Table 2. Irreducible representations (IRs) of $C_s = \{E, m\}$, $\overline{\Delta}_i$ are double valued.

	$\boldsymbol{\Delta_1}$	$\boldsymbol{\Delta_2}$	$\boldsymbol{\overline{\Delta}_3}$	$\boldsymbol{\overline{\Delta}_4}$
$\boldsymbol{E}$	***1***	***1***	***1***	***1***
$\boldsymbol{m}$	***1***	***-1***	$\boldsymbol{-i}$	$\boldsymbol{i}$
$\boldsymbol{\overline{E}}$	***1***	***1***	***-1***	***-1***
$\boldsymbol{\overline{m}}$	***1***	***-1***	$\boldsymbol{i}$	$\boldsymbol{-i}$

Supplementary Table 3. Irreducible representations (IRs) of $C_1 = \{E\}$, $\overline{\Delta}_i$ is double valued.

	$\boldsymbol{\Delta_1}$	$\boldsymbol{\overline{\Delta}_2}$
$\boldsymbol{E}$	**1**	**1**
$\boldsymbol{\overline{E}}$	**1**	**-1**

Supplementary Figures

Supplementary Figure 1. The AFE-FE path of TMCM-$MnCl_3$ as a function of the factor λ. (a) Top view of AFE state (λ=0), (b) Top view of intermediate state (λ=0.5), and (c) Top view of FE state (λ=1). (e) Side view of AFE state (λ=0), (f) Side view of intermediate state (λ=0.5), and (g) Side view of FE state (λ=1). The rotation axis of organic cation is along [010] direction, *i.e. b* axis. For easy visualization, the inorganic frameworks and some overlapping cations are not displayed in Fig. (e)-(g).

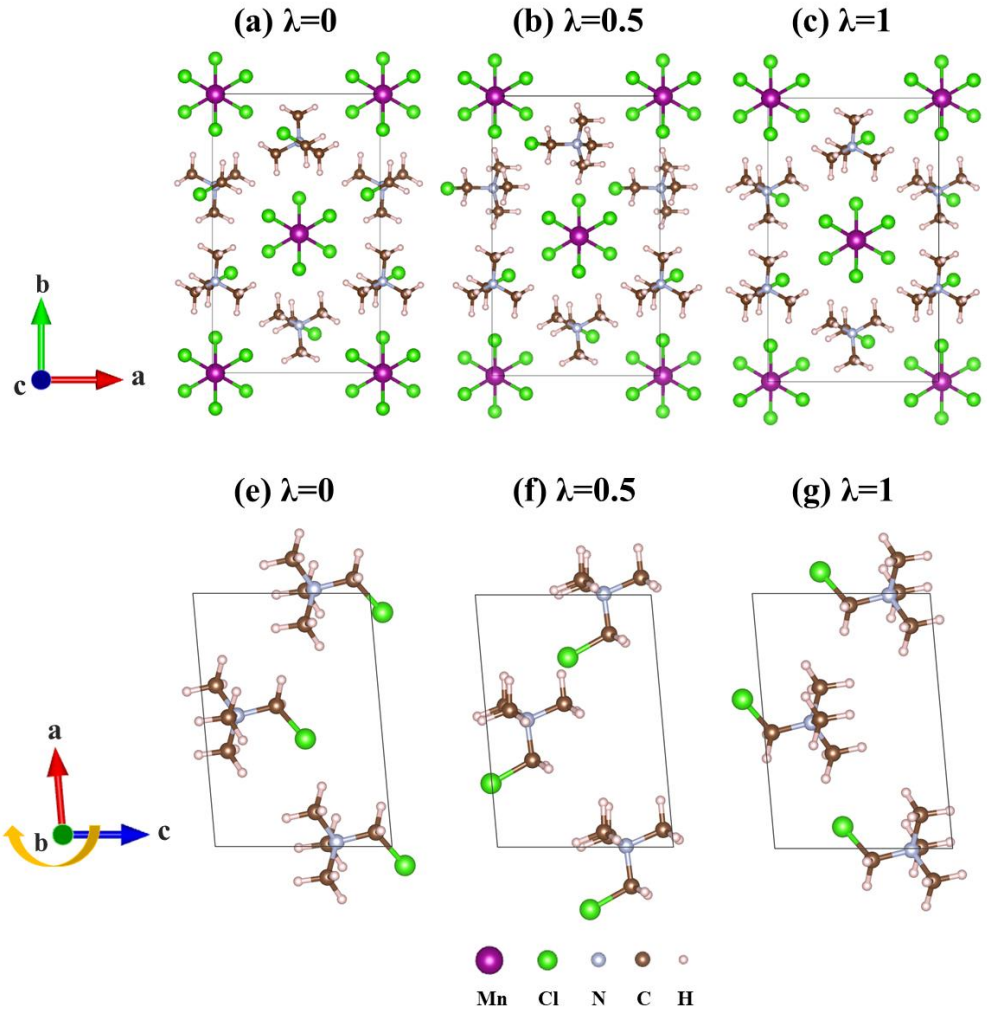

Supplementary Figure 2. (a) The polarization of $(Me_3NCH_2Cl)MnCl_3$ as a function of parameter λ. (b) The polarization of $(Me_3NCH_2Cl)MnY_3$, where Y = F, Cl, Br or I. (c) The polarization of $(Me_3NCH_2X)MnCl_3$, where X = F, Cl, Br or I. (d) The polarization of $(Me_3NCH_2X)MnY_3$, where X = Y = F, Cl, Br or I. P_x , P_z represent polarization in the *x*, *z* direction, respectively. P_{tot} represents the total polarization.

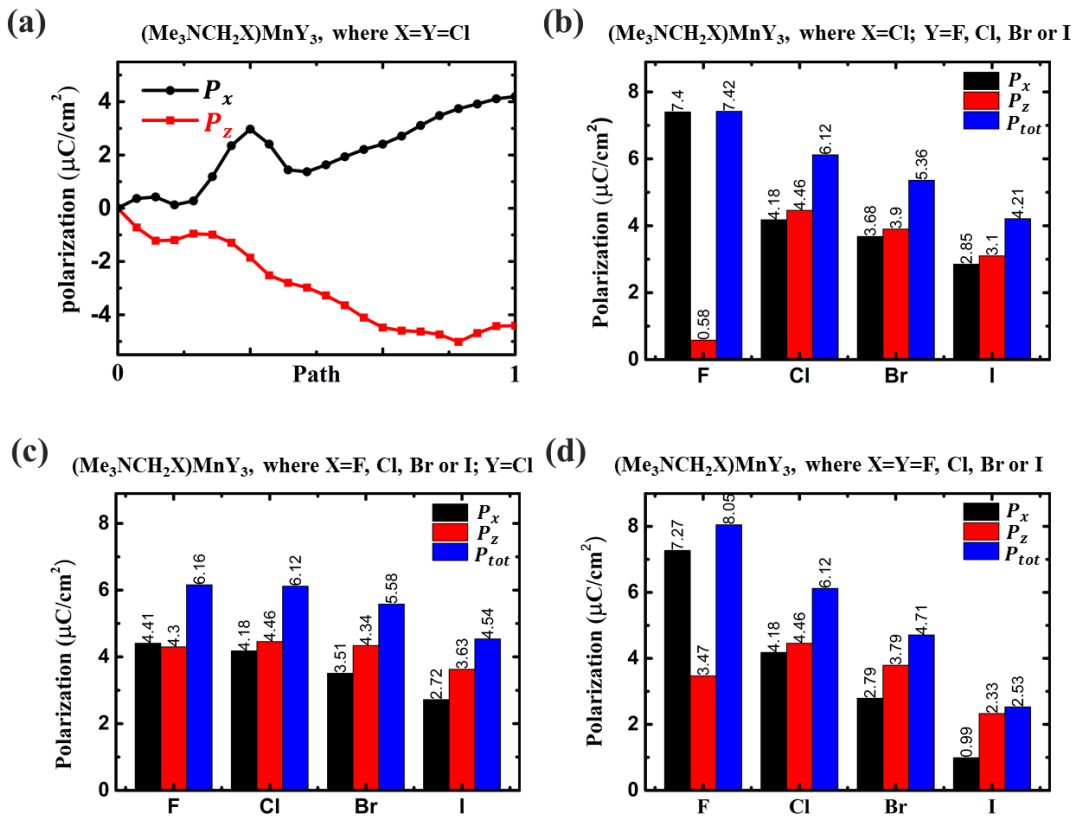

Supplementary Figure 3. The contributions of polarization in $(Me_3NCH_2X)MnCl_3$ (where X = F, Cl, Br and I). In (a), the lattice is fixed to the that of optimized $(Me_3NCH_2Cl)MnCl_3$. In (b), the lattice freely is optimized. The P_{ABX_3} is the total polarization, P_A is the polarization contributed by the dipole of organic cations, and P_{BX_3} is the polarization contributed by distortion of the inorganic framework.

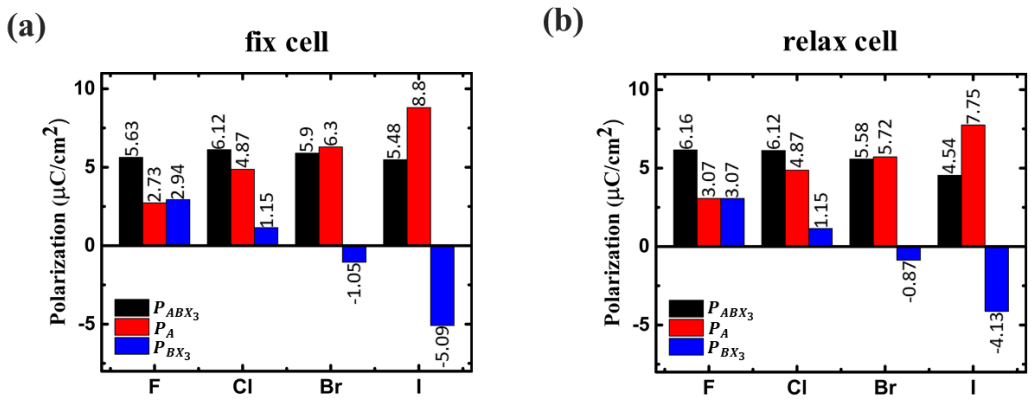

Supplementary Figure 4. Total energies of different magnetic states for TMCM-$MnCl_3$ *Cc* phase. The red arrows represent the directions of magnetic moments. Here, we do not consider SOC. As we can see, TMCM-$MnCl_3$ has strong AFM interaction within the inorganic $MnCl_3$ chains, while the interchain interaction is small. The G-type AFM state is the ground state and C-type AFM state has higher energy about 0.1 meV/Mn. Considering the weak interchain magnetic couplings, one can apply external fields (e.g., magnetic field) to switch the spins along one direction, *i.e.* C-type AFM state, thus C-type AFM state is common in experiments.

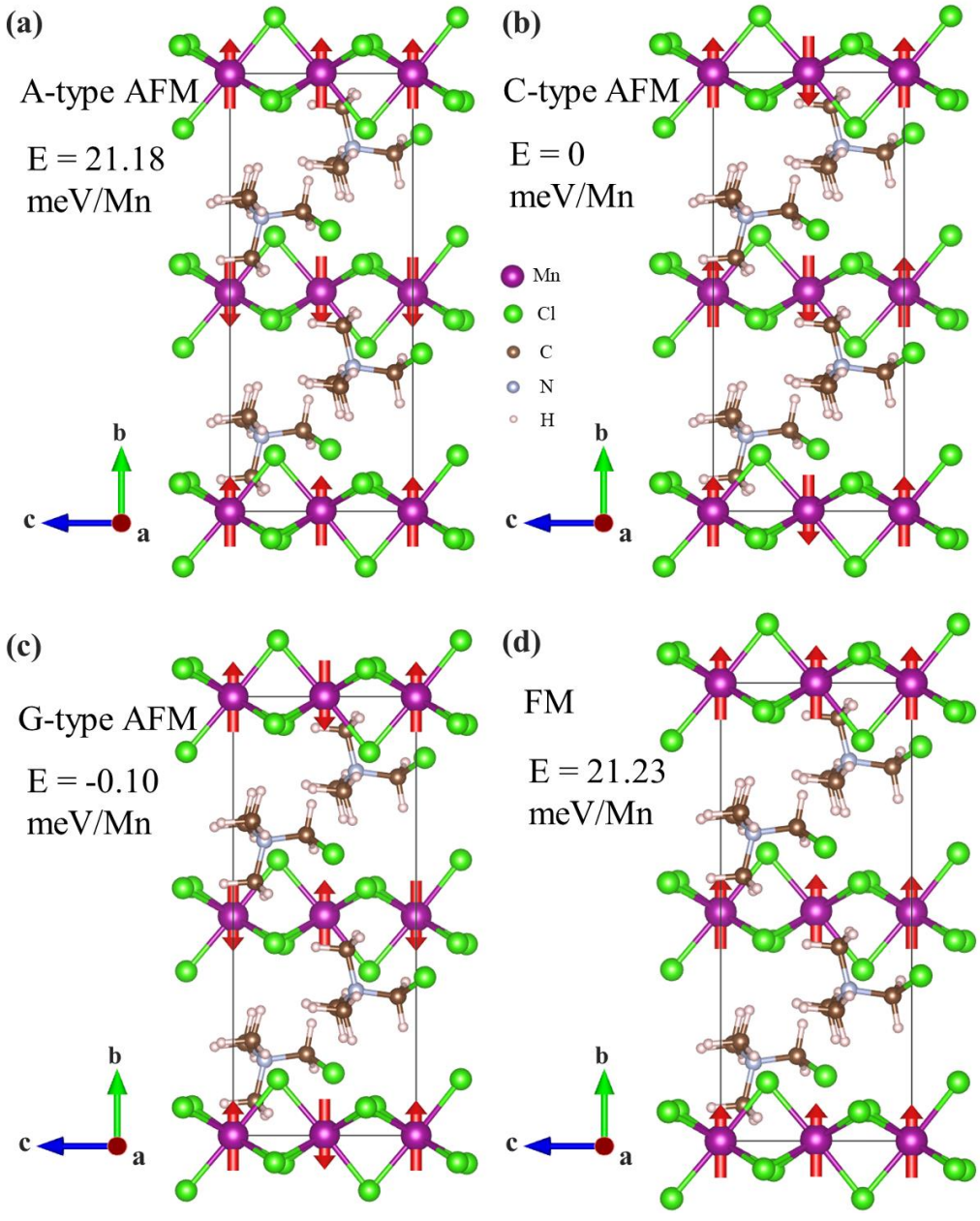

Supplementary Figure 5. The partial density of states (DOS) of G-type AFM state. The Fermi level is set to 0 eV. We can see that the valence band edge contains contributions from Mn-3*d* and Cl-2*p* orbitals, while the conduction band edge arises mainly from Mn-3*d* orbitals.

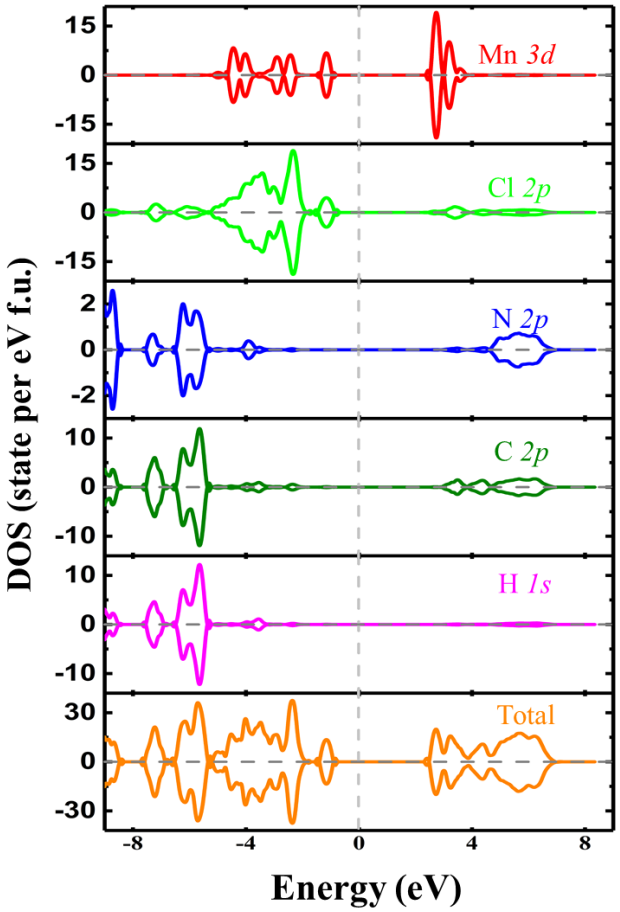

Supplementary Figure 6. The band structures without SOC (a) and with SOC (b-d) for G-type AFM$_x$, AFM$_{xz}$, and AFM$_z$ states, respectively. The abscissa is the Brillouin zone coordinate, and the ordinate is the energy, where the Fermi level is set to 0 eV. The magnified inset in (b-d) shows the SOC-induced band splitting around Γ point. The band degeneracy at Γ point is represented by $\bar{\mathrm{D}}$. The crystal lattice accompanied with the mirror reflection are shown in (e) with the polarization along approximately [10$\bar{1}$] direction. In (f), the first Brillouin zone with the symmetry path in band structure calculations.

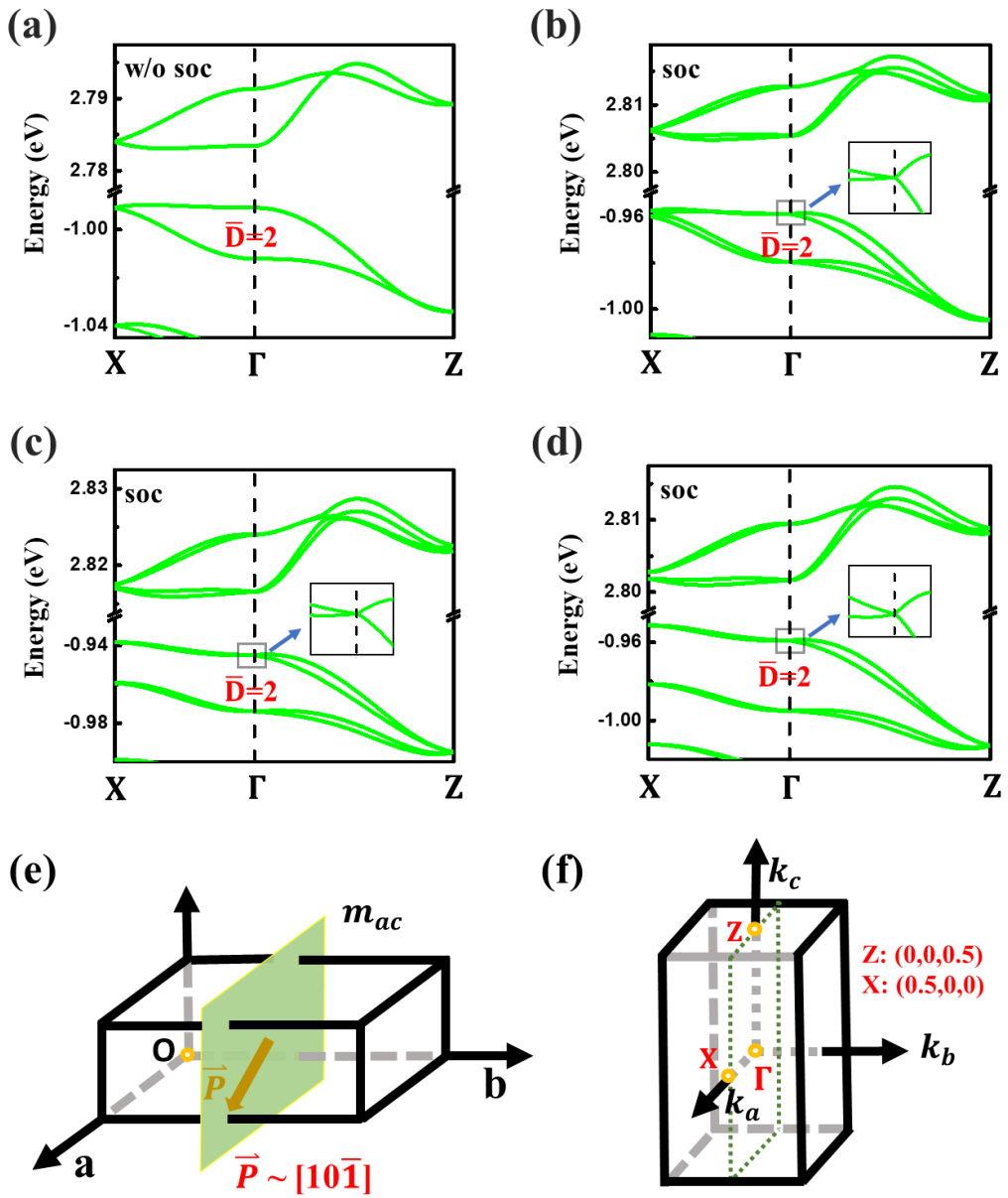

Supplementary Figure 7. The spin textures for G-type AFM$_x$. The polarization (p) is along the [$10\bar{1}$] direction. $\mathbf{L_G}$**~ x** denotes G-type AFM state with antiferromagnetic order parameter (**L**) along x direction. The arrows refer to the in-plane orientation of spin and the scale is shown in the top left corner, while colors indicate the out-of-plane component. (a) The spin texture near the outer VBM. (b) The spin texture near the inner VBM. (c) The spin texture near the inner CBM. (d) The spin texture near the outer CBM.

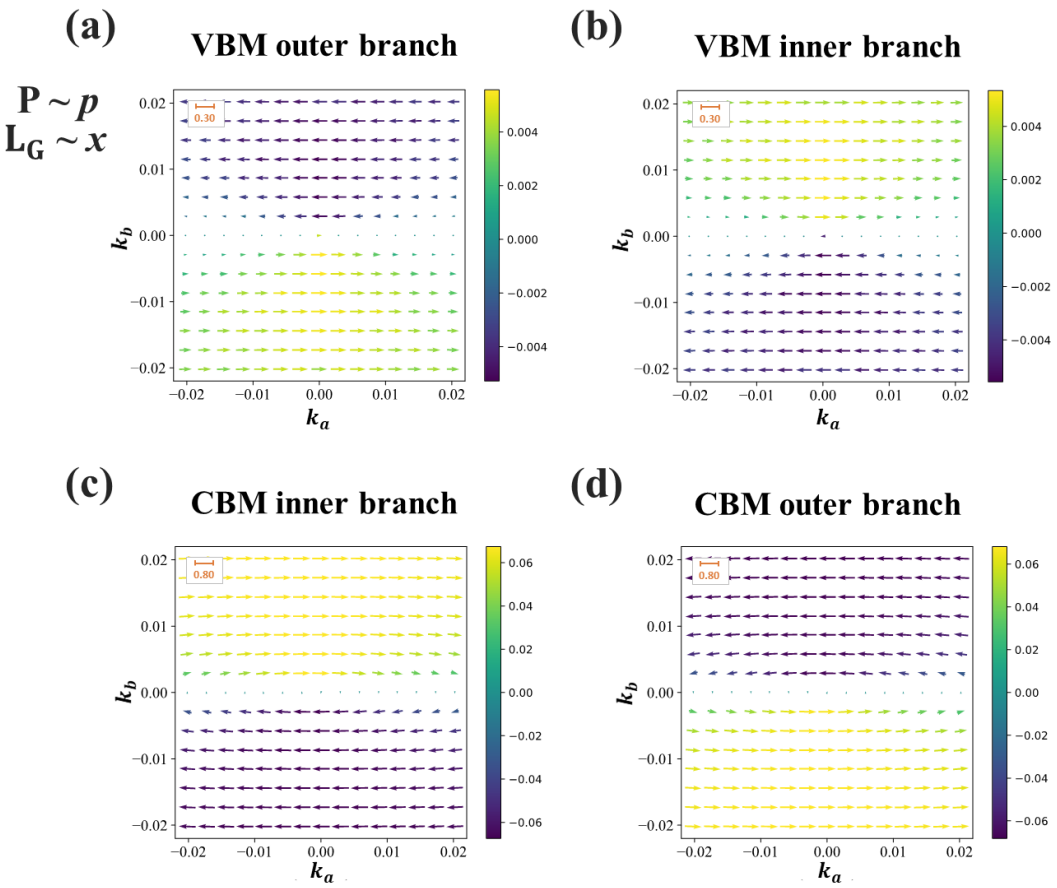

Supplementary Figure 8. The spin textures for G-type AFM$_{xz}$. The polarization (p) is along the [$10\bar{1}$] direction. $\mathbf{L_G}$ **~ xz** denotes G-type AFM state with antiferromagnetic order parameter (**L**) along xz direction. The arrows refer to the in-plane orientation of spin and the scale is shown in the top left corner, while colors indicate the out-of-plane component. (a) The spin texture near the outer VBM. (b) The spin texture near the inner VBM. (c) The spin texture near the inner CBM. (d) The spin texture near the outer CBM.

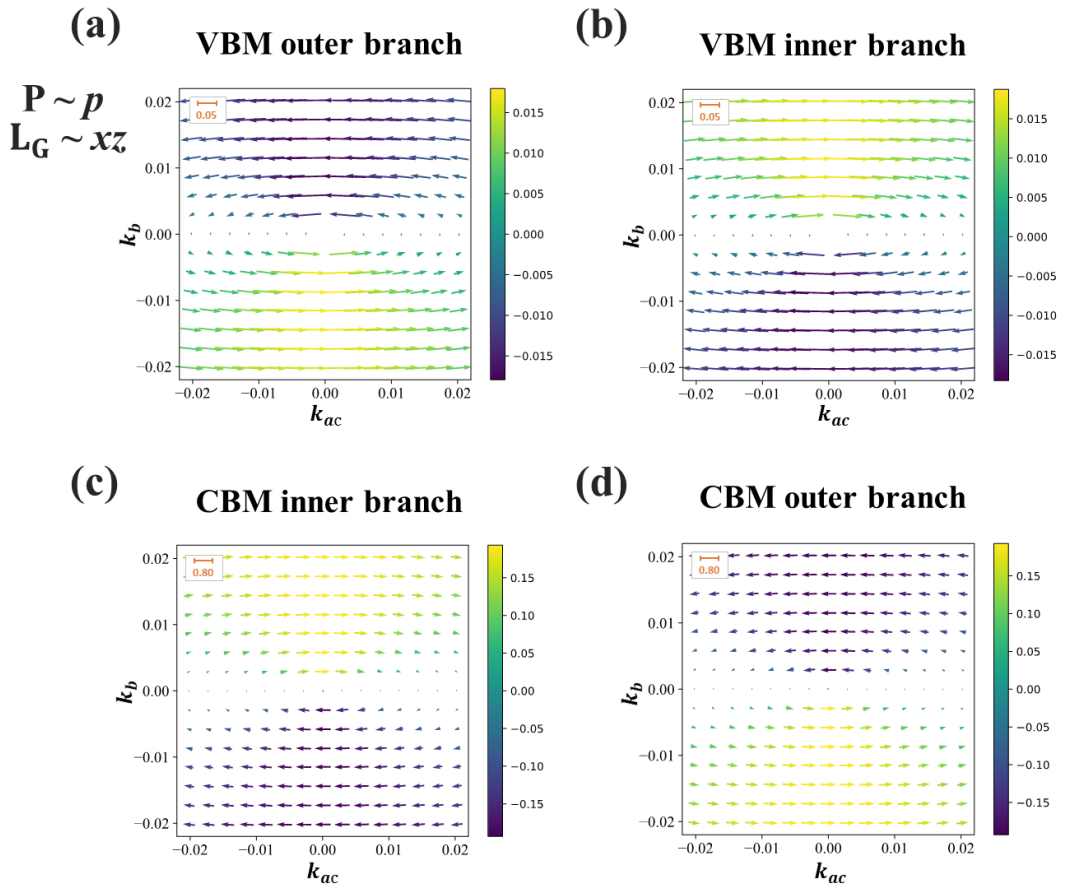

Supplementary Figure 9. The spin textures for G-type AFM$_z$. The polarization (p) is along the [10$\bar{1}$] direction. $\mathbf{L_G}$**~** $\boldsymbol{z}$ denotes G-type AFM state with antiferromagnetic order parameter (**L**) along z direction. The arrows refer to the in-plane orientation of spin and the scale is shown in the top left corner, while colors indicate the out-of-plane component. (a) The spin texture near the outer VBM. (b) The spin texture near the inner VBM. (c) The spin texture near the inner CBM. (d) The spin texture near the outer CBM.

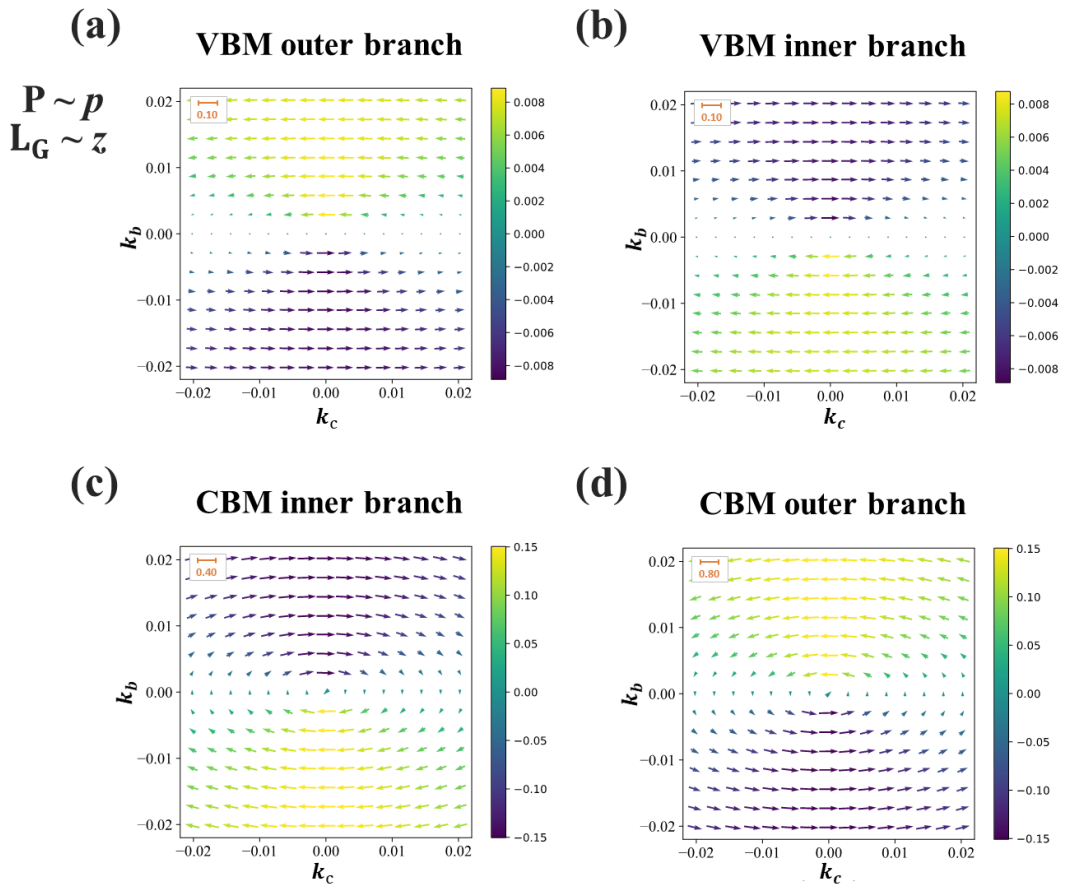

Supplementary Figure 10. The spin textures of TMCM-$MnCl_3$. The polarization (p) is along the $[10\bar{1}]$ direction. $\mathbf{L_G} \sim y$ denotes G-type AFM state with antiferromagnetic order parameter ($\mathbf{L}$) along y direction. The arrows refer to the in-plane orientation of spin and the scale is shown in the top left corner, while colors indicate the out-of-plane component. (a) The spin texture near the outer VBM. (b) The spin texture near the inner VBM. (c) The spin texture near the inner CBM. (d) The spin texture near the outer CBM.

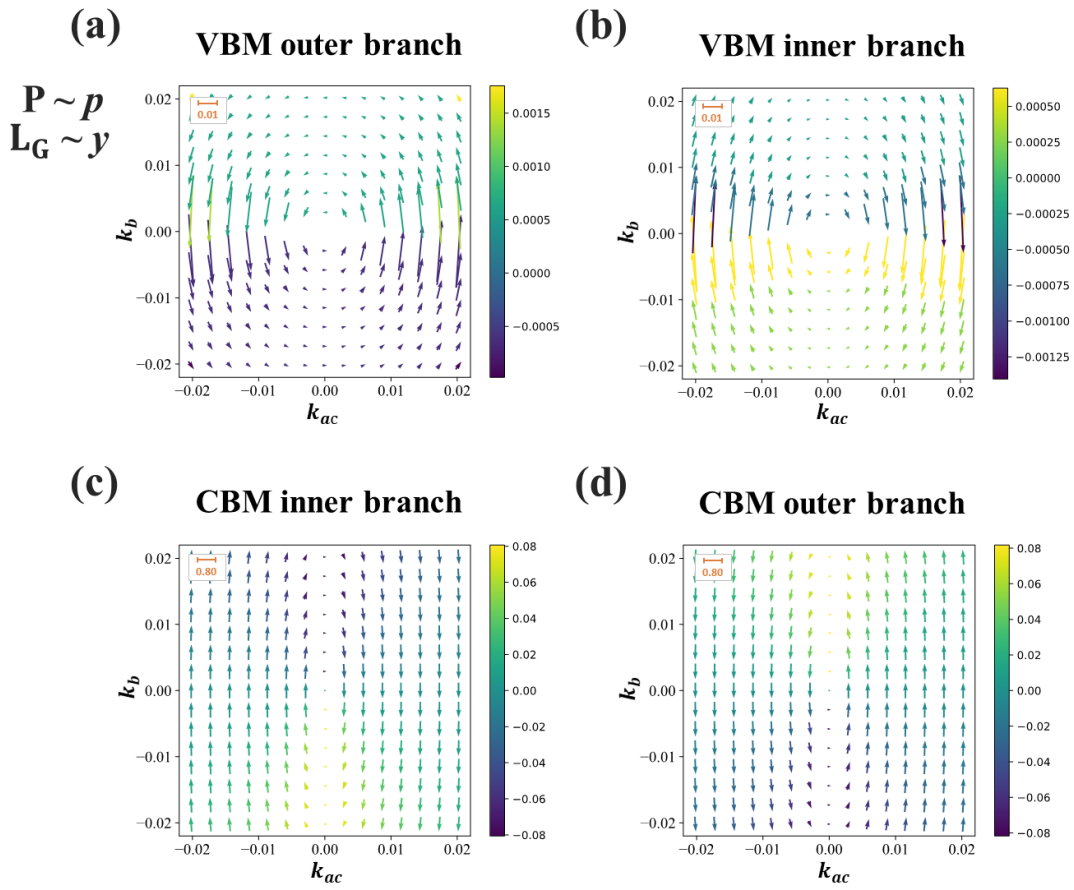

Supplementary Figure 11. The spin textures of TMCM-$MnCl_3$. The polarization (-*p*) is along the [$\bar{1}$01] direction. $\mathbf{L_G}$~***y*** denotes G-type AFM state with antiferromagnetic order parameter (**L**) along *y* direction. The arrows refer to the in-plane orientation of spin and the scale is shown in the top left corner, while colors indicate the out-of-plane component. (a) The spin texture near the outer VBM. (b) The spin texture near the inner VBM. (c) The spin texture near the inner CBM. (d) The spin texture near the outer CBM.

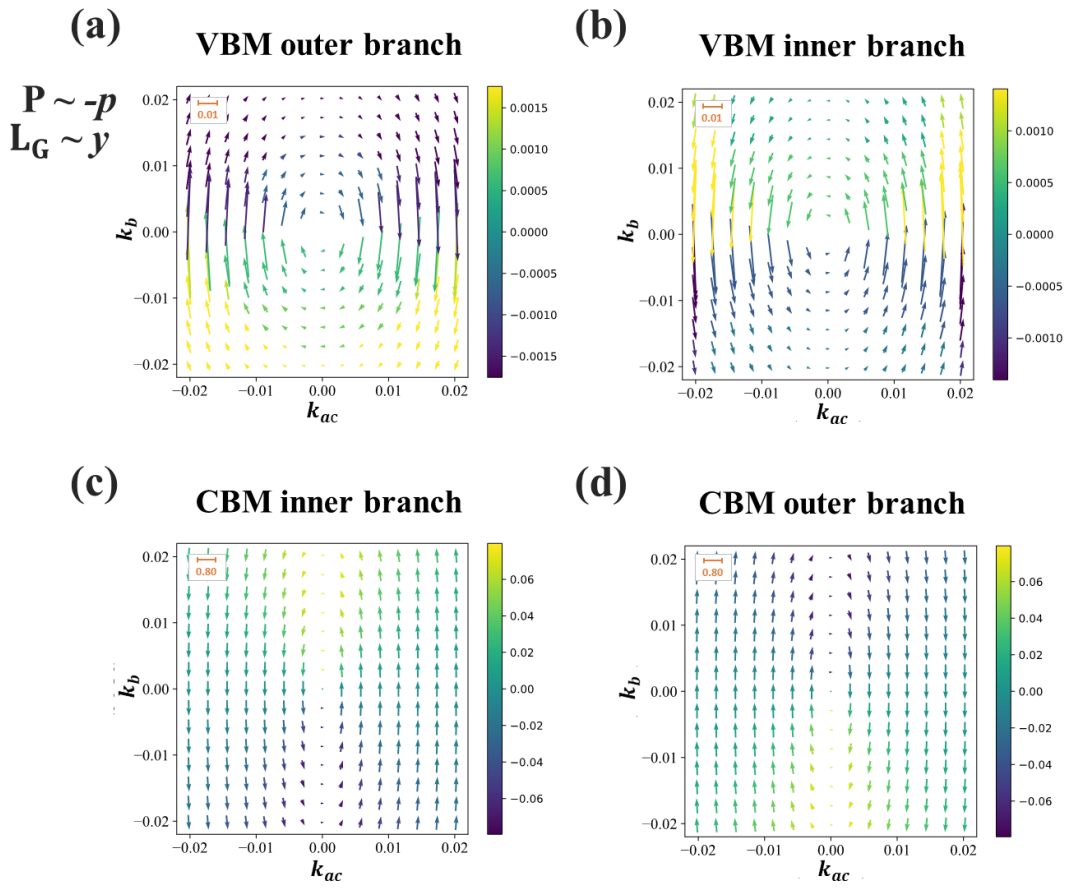

Supplementary Figure 12. The spin textures of TMCM-$MnCl_3$. The polarization (p) is along the [$10\bar{1}$] direction. $\mathbf{L_G}$**~ -*y*** denotes G-type AFM state with antiferromagnetic order parameter (**L**) along -y direction. The arrows refer to the in-plane orientation of spin and the scale is shown in the top left corner, while colors indicate the out-of-plane component. (a) The spin texture near the outer VBM. (b) The spin texture near the inner VBM. (c) The spin texture near the inner CBM. (d) The spin texture near the outer CBM.

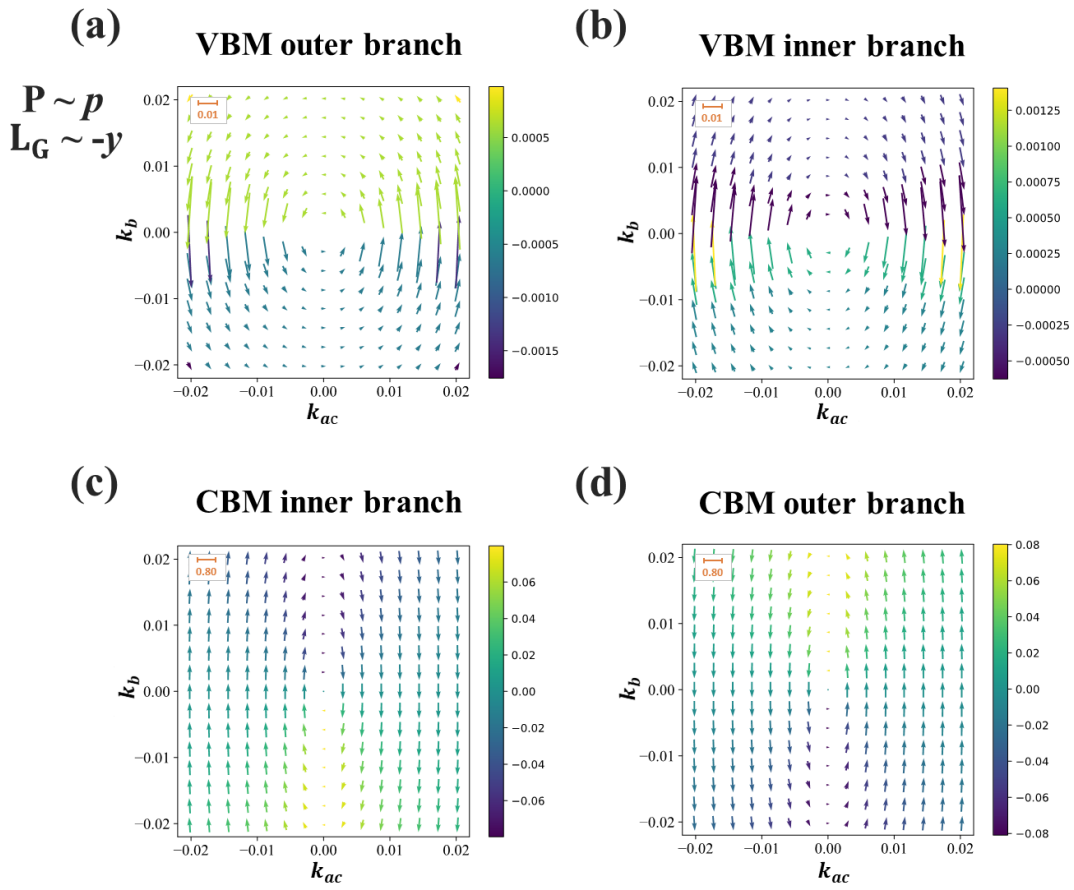

Supplementary Figure 13. The spin textures of TMCM-$MnCl_3$. The polarization (p) is along the [$10\bar{1}$] direction. $\mathbf{L_C} \sim y$ denotes C-type AFM state with antiferromagnetic order parameter (**L**) along y direction. The arrows refer to the in-plane orientation of spin and the scale is shown in the top left corner, while colors indicate the out-of-plane component. (a) The spin texture near the outer VBM. (b) The spin texture near the inner VBM. (c) The spin texture near the inner CBM. (d) The spin texture near the outer CBM.

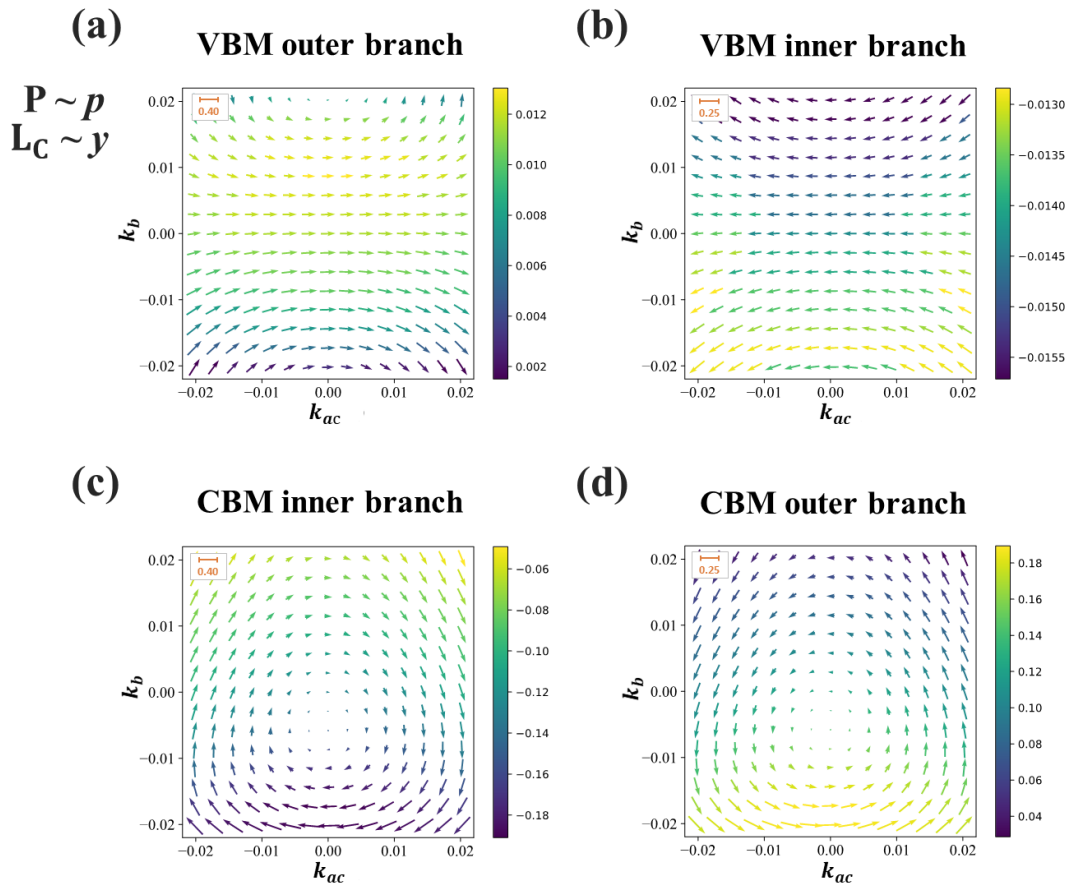

Supplementary Figure 14. The spin textures of TMCM-$MnCl_3$. The polarization (-*p*) is along the [$\bar{1}$01] direction. $\mathbf{L_C}$**~** ***y*** denotes C-type AFM state with antiferromagnetic order parameter (**L**) along *y* direction. The arrows refer to the in-plane orientation of spin and the scale is shown in the top left corner, while colors indicate the out-of-plane component. (a) The spin texture near the outer VBM. (b) The spin texture near the inner VBM. (c) The spin texture near the inner CBM. (d) The spin texture near the outer CBM.

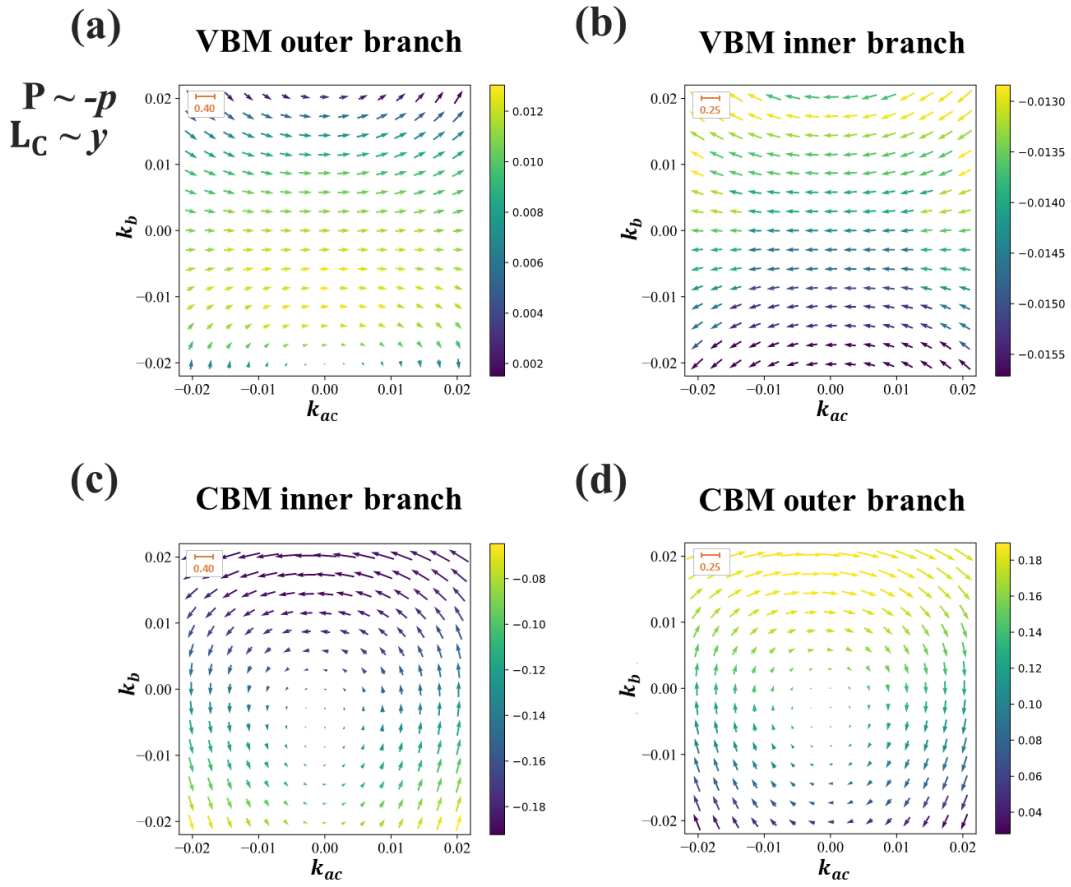

Supplementary Figure 15. The spin textures of TMCM-$MnCl_3$. The polarization (p) is along the [$10\bar{1}$] direction. $\mathbf{L_C}$**~ -*y*** denotes C-type AFM state with antiferromagnetic order parameter (**L**) along -y direction. The arrows refer to the in-plane orientation of spin and the scale is shown in the top left corner, while colors indicate the out-of-plane component. (a) The spin texture near the outer VBM. (b) The spin texture near the inner VBM. (c) The spin texture near the inner CBM. (d) The spin texture near the outer CBM.

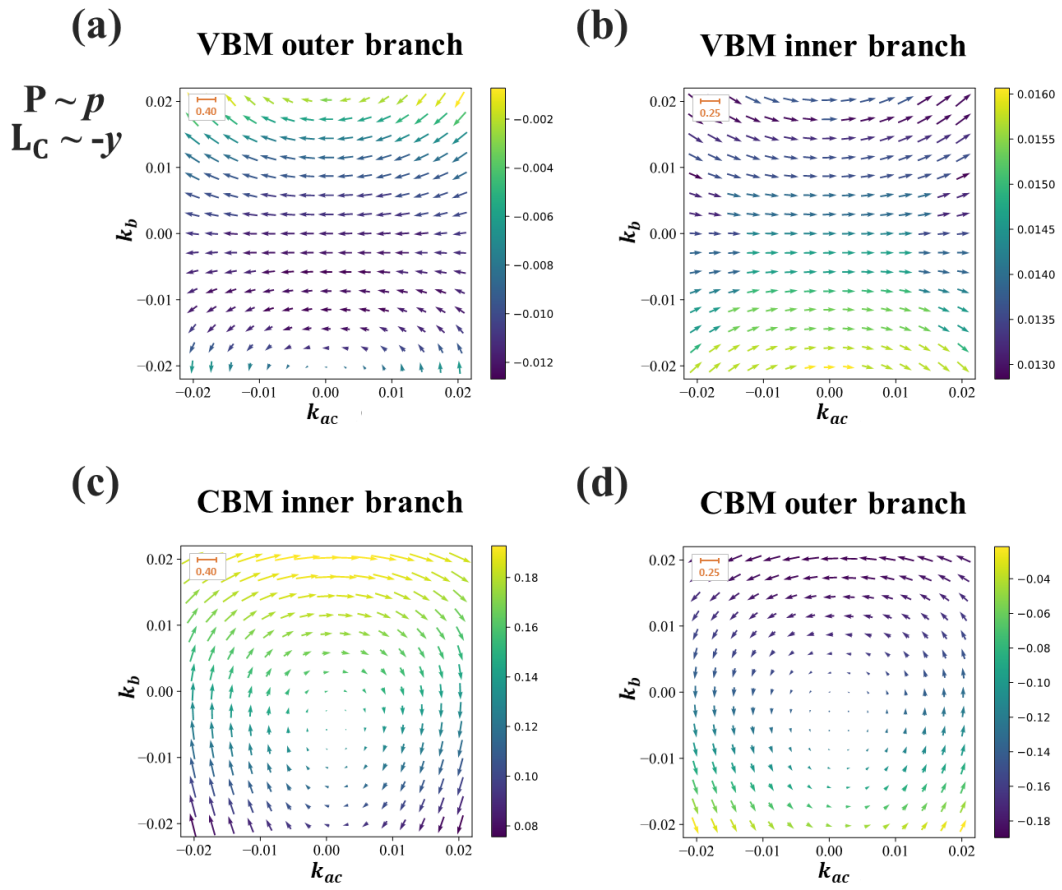

Supplementary Figure 16. The spin textures of TMCM-$MnCl_3$. The polarization (p) is along the [$10\bar{1}$] direction. $\mathbf{L_C} \sim z$ denotes C-type AFM state with antiferromagnetic order parameter ($\mathbf{L}$) along z direction. The arrows refer to the in-plane orientation of spin and the scale is shown in the top left corner, while colors indicate the out-of-plane component. (a) The spin texture near the outer VBM. (b) The spin texture near the inner VBM. (c) The spin texture near the inner CBM. (d) The spin texture near the outer CBM.

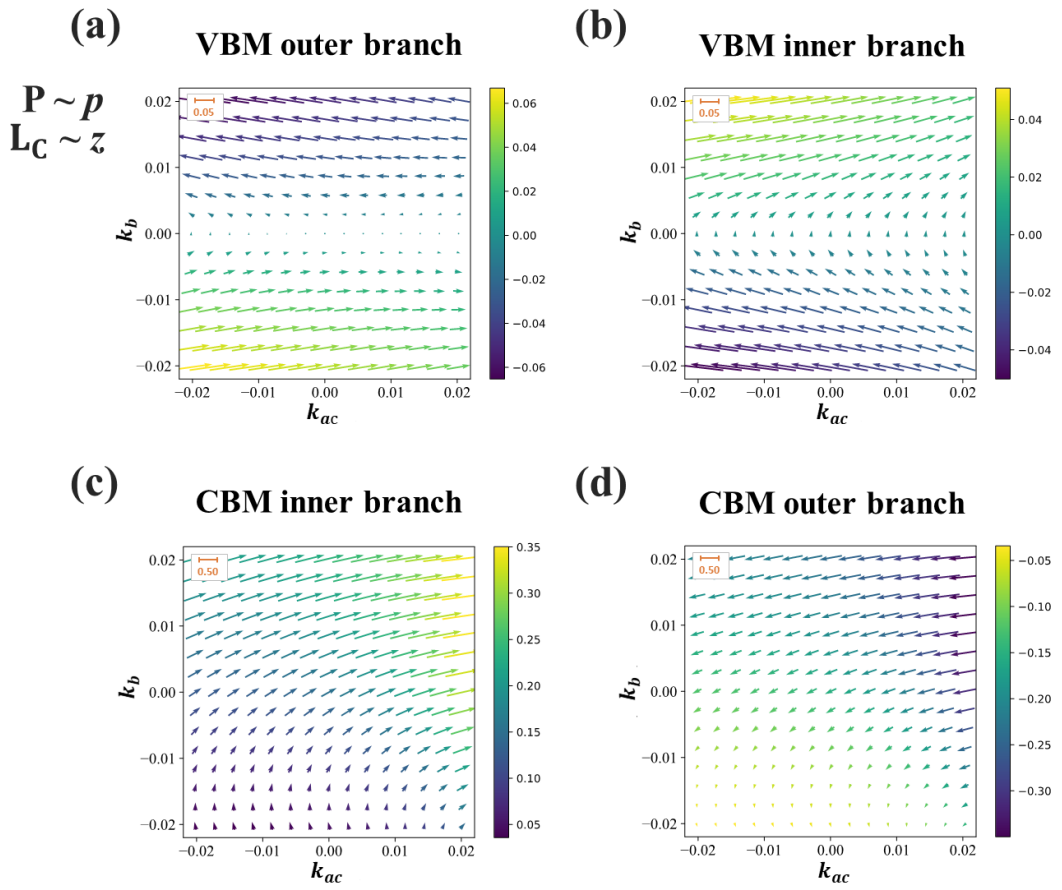

Supplementary Figure 17. The spin textures of TMCM-$MnCl_3$. The polarization (p) is along the [$10\bar{1}$] direction. $\mathbf{L_F}$**~** $\boldsymbol{y}$ denotes FM state along y direction. The arrows refer to the in-plane orientation of spin and the scale is shown in the top left corner, while colors indicate the out-of-plane component. (a) The spin texture near the outer VBM. (b) The spin texture near the inner VBM. (c) The spin texture near the inner CBM. (d) The spin texture near the outer CBM.